



Improved waste-sourced biocomposite for simultaneous removal of crude oil and heavy metals from synthetic and real oilfield-produced water

Razegheh Akhbarizadeh¹ · Farid Moore¹ · Dariush Mowla² · Behnam Keshavarzi¹

Received: 17 June 2018 / Accepted: 3 September 2018 / Published online: 8 September 2018
© Springer-Verlag GmbH Germany, part of Springer Nature 2018

Abstract

Oil- and gas-produced water (PW) which contains various pollutants is an enormous threat to the environment. In this study, a novel low-cost bio-adsorbent was prepared from shrimp shell and acid-activated montmorillonite. The results of FT-IR spectroscopy, energy dispersive X-ray (EDX) analysis, and SEM-EDX technique indicated that the chitosan-activated montmorillonite (CTS-A-MMT) was prepared successfully. The synthesized CTS-A-MMT was applied to remove simultaneously five cationic and anionic metal species and crude oil from synthetic and real oilfield PW. The adsorption data indicated that crude oil and all studied metals (except As) were adsorbed to CTS-A-MMT in a monolayer model (best fitted by Langmuir model), while As adsorption fits well with Freundlich model. Kinetic models' evaluation demonstrated that the adsorption kinetics of metals on CTS-A-MMT are initially controlled by the chemical reaction (film diffusion) followed by intra-particle diffusion. Application of the prepared CTS-A-MMT in real oilfield PW indicated removal efficiency of 65 to 93% for metals and 87% for crude oil in simultaneous removal experiments. Presence of additional ions in PW decreased the removal of studied metals and crude oil considerably; however, the concentration of the investigated pollutants in treated PW is less than the ocean discharge criteria. It is concluded that the prepared CTS-A-MMT composite is a low-cost and effective adsorbent for treating wastewater contaminated with crude oil and heavy metals (i.e., PW).

Keywords Oilfield-produced water · Chitosan-modified montmorillonite · Crude oil · Adsorption · Heavy metals · Treatment

Introduction

Oil- and gas-produced water (PW) is a byproduct of petroleum production (Fakhru'l-Razi et al. 2009; Shpiner et al. 2009b). Physical and chemical properties of PW can be affected by various parameters including geological setting of the field,

reservoir characteristics, reservoirs lifetime, characteristics of the hydraulic fracturing process, hydrocarbon types, operational conditions, and the used additives (Fakhru'l-Razi et al. 2009; Olsson et al. 2013). The brine to oil-produced ratio is 2:1 for conventional oil wells, while it is 35% less for unconventional wells (Farag and Harper 2014; Phan et al. 2015). The salinity of PW is also much higher for conventional reservoirs compared with that for unconventional ones (for example, average total-dissolved solids in PWs from conventional Devonian age reservoirs in Pennsylvania and West Virginia are reported to be 165 g/L, while it is 25.3 g/L for Marcellus Shale) (Skalak et al. 2014). However, PWs from unconventional reservoirs tend to exhibit high concentrations of Sr, Ba, and Ra relative to conventional wells (Skalak et al. 2014). For instance, the range of Ba in conventional reservoir PW is from a few mg/L to 4370 mg/L, but brine from unconventional wells ranges from 76 to 13,600 mg/L (Phan et al. 2015; Skalak et al. 2014). Similarly, the concentration of Ra in PWs from Marcellus is 2–5 times higher than conventional

Responsible editor: Tito Roberto Cadaval Jr

Electronic supplementary material The online version of this article (<https://doi.org/10.1007/s11356-018-3136-2>) contains supplementary material, which is available to authorized users.

✉ Razegheh Akhbarizadeh
akhbarizade@shirazu.ac.ir

¹ Department of Earth Sciences, College of Science, Shiraz University, Shiraz 71454, Iran

² School of Chemical and Petroleum Engineering, Shiraz University, Mollasadra Ave., Shiraz 71345, Iran

reservoirs for a given salinity (Skalak et al. 2014). Regardless of reservoirs type, PWs usually contain various pollutants including oil and grease, salt, chemical additives, organic and inorganic compounds, and natural radioactive material (Shpiner et al. 2009a; Torres et al. 2017; Venkatesan and Wankat 2017). Due to the relatively high concentration of toxic pollutants in PW, its direct discharge to the environment may pose a threat to biota and human health (Torres et al. 2017). Despite the fact that PW management presents environmental challenges and high cost (Venkatesan and Wankat 2017), but in semi-arid regions (such as Middle East), due to water scarcity, treatment and reuse of PW for different purposes is economically justified (Shpiner et al. 2009b). Electrocoagulation, pH adjustment, hydrocyclone, microfiltration, centrifugation, membrane filter, and bioremediation are common methods used to remove pollutants from PW. However, problem of additives, high retention times, and high cost may limit such applications (Arthur et al. 2005; Shpiner et al. 2009b; Venkatesan and Wankat 2017). Among the different treatment methods (physical, chemical, and biological), adsorption is the most promising method because of its eco-compatibility, simplicity of operation, high efficiency, and cost-effectiveness (Pawar et al. 2016; Zhang et al. 2016).

Chitosan (poly- β -(1,4)-2-amino-2-deoxy-glucopyranose, CTS) is one of the most promised adsorbents due to its high adsorption capacity, low cost, nontoxicity, abundance, biodegradability, and biocompatibility (Azzam et al. 2016; da Costa et al. 2016; Dotto et al. 2016; Wang et al. 2014a). However, some shortcomings such as poor selective adsorption, low acid and thermal stability, low porosity, small specific surface area, and mechanical strength restrict chitosan application (Wang et al. 2014a; Zhang et al. 2016). As a result, many researchers have applied different modifications to resolve these weaknesses and enhance chitosan adsorption capacity (Azzam et al. 2016; da Costa et al. 2016; El-Dib et al. 2016; Negm et al. 2015).

Over the past few decades, clay minerals mostly due to their large surface area, chemical and mechanical stability, high cation exchange capacity, availability, nontoxicity, and low cost are widely used in environmental applications such as pollution control (Djukić et al. 2013; Hadjltaief et al. 2018). Montmorillonite (MMT) is a 2:1 layered aluminosilicate of smectite-type clay mineral comprised of two tetrahedral sheets of silica sandwiching a central octahedral sheet of Al (Iler 1979; Pawar et al. 2016). Generally, the substitution of Mg^{2+} for Al^{3+} makes the layers negatively charged (Hu et al. 2016). The presence of exchangeable cations such as alkali or alkaline earth metal cations in the interlayer space neutralizes the negative charge (Pawar et al. 2016; Wang et al. 2014a). Properties such as abundance, low cost, high specific surface and porosity, eco-friendliness, and interlayer cation exchangeability make MMT a good candidate as an adsorbent for water and wastewater treatment (Pawar et al. 2016; Taha et al. 2016;

Wang et al. 2014a). Acid activation is an effective way of enhancing the physical and chemical properties of clay minerals including increased porosity, specific surface, and subsequently their adsorption capacity (Azzam et al. 2016; de Queiroga et al. 2016; Pawar et al. 2016; Stawinski et al. 2016). A combination of acid-activated MMT and chitosan was thought to improve their adsorption capability.

Various researchers focused on simultaneous removal of pollutants by chitosan-based adsorbent during the last decades (Chen et al. 2018; Doshi et al. 2018; Pawar et al. 2016; Vieira et al. 2018). However, few studies have reported the simultaneous removal of cationic and anionic species (Luo et al. 2015; Sargin et al. 2015; Shankar et al. 2014; Song et al. 2018). Neither of these publications has studied the simultaneous removal of five cationic and anionic species nor crude oil from synthetic aqueous solution and real oilfield-produced water. Hence, the aim of the current research was to (1) prepare a microsized chitosan-activated montmorillonite (CTS-A-MMT); (2) investigate the adsorbing ability for competitive removal of Mn (II), Ba (II), As (III), V (V), Cr (VI), and crude oil from a synthetic solution under various physicochemical parameters; and (3) determine the ability of CTS-A-MMT to eliminate oil and selected heavy metals from PW.

Materials and methods

Materials and chemicals

Shrimp shells were purchased from a local fishmonger in Bushehr harbor, SW Iran. The raw Na-montmorillonite powder ($< 45 \mu m$) with a cation exchange capacity of 86 meq/100 g was purchased from Zaminkav Co., Iran. All chemicals were analytical grade and supplied by Merck Co. All laboratory glassware was washed with 30% HNO_3 , rinsed with deionized water, and dried in an oven. Sample bottles were washed with tap water, rinsed with deionized water, and let to dry.

Preparation of chitosan-activated montmorillonite composite (CTS-A-MMT)

In the first step, chitosan with 86.92% degree of deacetylation was prepared according to the method described by Du et al. (2009). Accordingly, shrimp shells were washed with tap water, dried at room temperature, and grinded. Then, 100.0 g of shrimp shell powder ($< 250 \mu m$) was immersed in 1000 mL of 7% (w/w) HCl for 24 h at 25 °C. The resultant slurry was filtered and washed with distilled water until neutral pH was reached. The residue was put into 1000 mL of 10% (w/w) NaOH for 24 h at 60 °C. After filtration, the residue was washed to neutrality in distilled water. All steps were repeated two times. The prepared chitin was oven-dried at 50 °C

overnight. In order to deacetylate the chitin, 10.0 g of dried chitin was immersed in 140 mL of 70% (w/w) NaOH for 6 h at 80 °C (stirring). The slurry was filtered and washed with hot distilled water (60 °C) to neutrality. The residue was oven-dried at 50 °C overnight.

In the next step, acid-activated MMT was prepared by immersing 10.0 g of MMT (< 45 μm) in 200 mL of 3 M HNO₃. The mixture was stirred at 500 rpm for 4 h at 80 °C. The activated clay was washed with distilled water to neutrality and left to dry with 105 °C for 24 h in an oven.

Finally, 1.0 g of the prepared chitosan was dissolved in 100 mL of 5% (v/v) acetic acid under vigorous stirring for 2 h at 60 °C. Then, 4.0 g of acid-activated MMT was added to the prepared chitosan gel and stirred at 350 rpm for 24 h at room temperature. The pH of the resultant slurry was neutralized using NaOH and then filtered and washed with distilled water. The obtained composite was dried in an oven at 60° for 24 h. The dried matter was grinded using mortar and pestle and screened through a 60-mesh (250 μm) sieve.

pH of point of zero charge (pH_{pzc})

In order to obtain the pH of the point of zero charge (pH_{pzc}) of CTS-A-MMT, 0.15 g aliquots of the adsorbent were put in beakers containing 50 mL of 0.01 M NaCl solution with pH of 3.0, 4.0, 5.0, 6.0, 7.0, and 8.0 (Pawar et al. 2016). The pH was adjusted previously by adding 0.1 M HCl and 0.1 M NaOH solution. The mixture was shaken vigorously at room temperature for 24 h, and then the pH of the solution was measured. After drawing the final pH versus initial pH, the point at which the final pH and initial pH are equal is the pH_{pzc} (Pawar et al. 2016).

Characterization of the chitosan-activated montmorillonite composite

A scanning electron microscope (SEM) coupled with an energy dispersive X-ray (EDX) was used to study the surface morphology and chemical composition of CTS, MMT, A-MMT, and the prepared CTS-A-MMT composite before and after treatment. The functional group of CTS, MMT, A-MMT, and prepared CTS-A-MMT composite before and after treatment was identified using a Fourier transform infrared spectrometer (FT-IR). The FT-IR spectra of samples ranged from 400 to 4000 cm⁻¹ at a resolution of 4 cm⁻¹. X-ray diffraction (XRD) analysis was performed to check CTS, MMT, A-MMT, and the prepared CTS-A-MMT composite, using Cu Kα radiation. The diffraction patterns were collected from 2° to 70° 2θ, and the scanning rate was 2°/min. The resulting intensities and peaks of each compound were compared with related files published by the international center for diffraction data.

Batch adsorption studies

All tests were carried out by changing initial metal concentration, pH, contact time, adsorbent dosage, and oil concentration. The competitive adsorption experiments of Mn (II), Ba (II), As (III), V (V), and Cr (VI) were carried out by adding 0.1 g of CTS-A-MMT into 50 mL of 10 mg/L metals solution for 24 h at room temperature. Equilibration was achieved using a mechanical shaker at 350 rpm. The effect of pH was investigated at pH of 4.0, 5.0, 6.0, 7.0, and 8.0. The pH levels were adjusted by adding 0.1 M HCl and 0.1 M NaOH solution. The initial concentration of metal solution ranged from 1 to 80 mg/L. The metals stock solutions (1000 mg/L) were prepared by dissolving Mn metal strip in nitric acid, As₂O₃ salt in NaOH, and K₂Cr₂O₇, NH₄VO₃, and BaCl₂.2H₂O salt in double-distilled water. Different concentrations of heavy metals were prepared by diluting stock solutions, using double-deionized water. Contact time effects were observed from 6 min to 24 h. Five different adsorbent doses were investigated. Moreover, the initial oil concentrations ranged from 600 to 1800 mg/L. The final treated solution was filtered using a 0.45 μm syringe filter and acidified. The metal concentration was measured using inductively coupled plasma mass spectrometry (ICP-MS). Furthermore, the USEPA method 1664 was used for quantification of oil and grease before and after treatment in samples that contained crude oil (USEPA 1999). All experiments were done two times in order to check the reliability of the adsorption process.

Three well-known isotherms (Freundlich, Langmuir, and Temkin) were used to investigate the sorption pattern. The nonlinear form of the isotherm models is given as:

$$q_e = K_f(C_e)^{1/n}$$

$$q_e = \frac{q_m K_l C_e}{1 + K_l C_e}$$

$$q_e = \frac{RT}{b_T} \ln(K_T C_e)$$

where, *q_e* is the adsorbed amount of metals (mg/g), *K_f* and 1/*n* are Freundlich constant parameters, *C_e* is the equilibrium concentration (mg/L), *q_m* is the monolayer capacity of the adsorbent (mg/g), *K_l* is affinity of adsorbent to adsorbate (L/g), *K_T* (L/mg) correlating the maximum binding energy, *R* is gas constant (8.314 J/mol K), *T* (K) is absolute temperature, and *b_T* (J/mol) is heat of adsorption (Auta and Hameed 2013; Pawar et al. 2016; Wang et al. 2014a).

The removal efficiency (*R*-%) and the adsorbed amount of metals after equilibrium (*q_e*-mg/g) were calculated using the following equations (Negm et al. 2015; Wang et al. 2014b):

$$q_e = (C_0 - C_e) \frac{V}{M}$$

Table 1 Elemental composition of chitosan (CTS), montmorillonite (MMT), activated montmorillonite (A-MMT), and chitosan-activated montmorillonite composite (CTS-A-MMT) in (wt%)

Elements	CTS	MMT	A-MMT	CTS-A-MMT
C	57.74	4.45	3.86	14.97
O	38.74	42.90	42.15	42.28
Na	–	1.10	0.42	0.43
Mg	0.47	0.78	0.55	0.54
Al	–	7.3	5.98	4.31
Si	–	31.71	33.79	33.71
K	–	1.16	0.55	0.54
Ca	–	2.70	0.45	–
Fe	–	7.88	5.65	–

$$R = \frac{(C_0 - C_e)}{C_0} \times 100$$

where, C_0 is initial concentration of metals in the solution (mg/L), C_e is metals concentration at equilibrium in the solution (mg/L), V is the volume of solution (L), and M is the mass of used adsorbent (g).

The pseudo-first-order, pseudo-second-order, and intra-particles diffusion kinetic models were used to determine the best model to describe adsorption of metals on CTS-A-MMT (Wang et al. 2014a). The nonlinear form of equations is as follows, respectively:

$$q_t = q_e(1 - e^{-k_1 t})$$

$$q_t = \frac{k_2 q_e^2 t}{(1 + k_2 q_e t)}$$

$$q_t = k_i t^{\frac{1}{2}} + C_i$$

where, q_e and q_t are adsorbed metals (mg/g) at equilibrium and time (t-min), respectively. k_1 (min^{-1}), k_2 ($\text{g}/\text{mg}\cdot\text{min}$), and k_i ($\text{mg}/(\text{g}\cdot\text{min}^{0.5})$) are the rate constants of the pseudo-first-order, pseudo-second-order, and intra-particle diffusion kinetic model, respectively (Auta and Hameed 2013; Wang et al. 2014a). C_i is the thickness of the boundary layer (Futalan et al. 2011).

Results and discussions

Adsorbent composition and characterization

SEM-EDX analysis

The surface morphology and chemical composition of raw materials and the composite were determined using SEM-EDX. The elemental composition of CTS, MMT, A-MMT, and CTS-A-MMT is shown in Table 1. As only C (57.74 wt%), O (38.74 wt%), and Mg (0.47 wt%) were detected in CTS, the cells for other element remained blank in the table. Si and O are major elements in MMT and A-MMT, while CTS-A-MMT is mostly composed of O, Si, and C. Moreover, SEM images (Fig. 1) show that the irregular and flaky particles of CTS have a rough surface (Fig. 1a). The agglomerated particles of MMT display

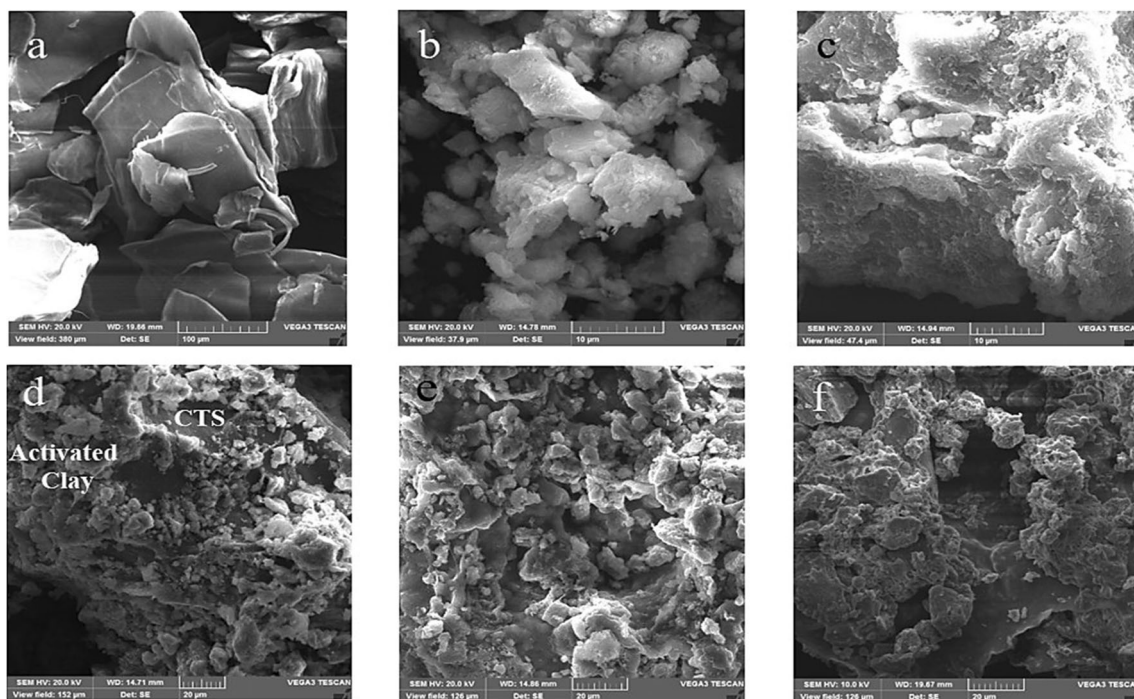


Fig. 1 SEM images. **a** Chitosan. **b** Montmorillonite. **c** Activated montmorillonite. **d** Chitosan-activated montmorillonite before adsorption. **e** Chitosan-activated montmorillonite after metal adsorption. **f** Chitosan-activated montmorillonite after oil adsorption

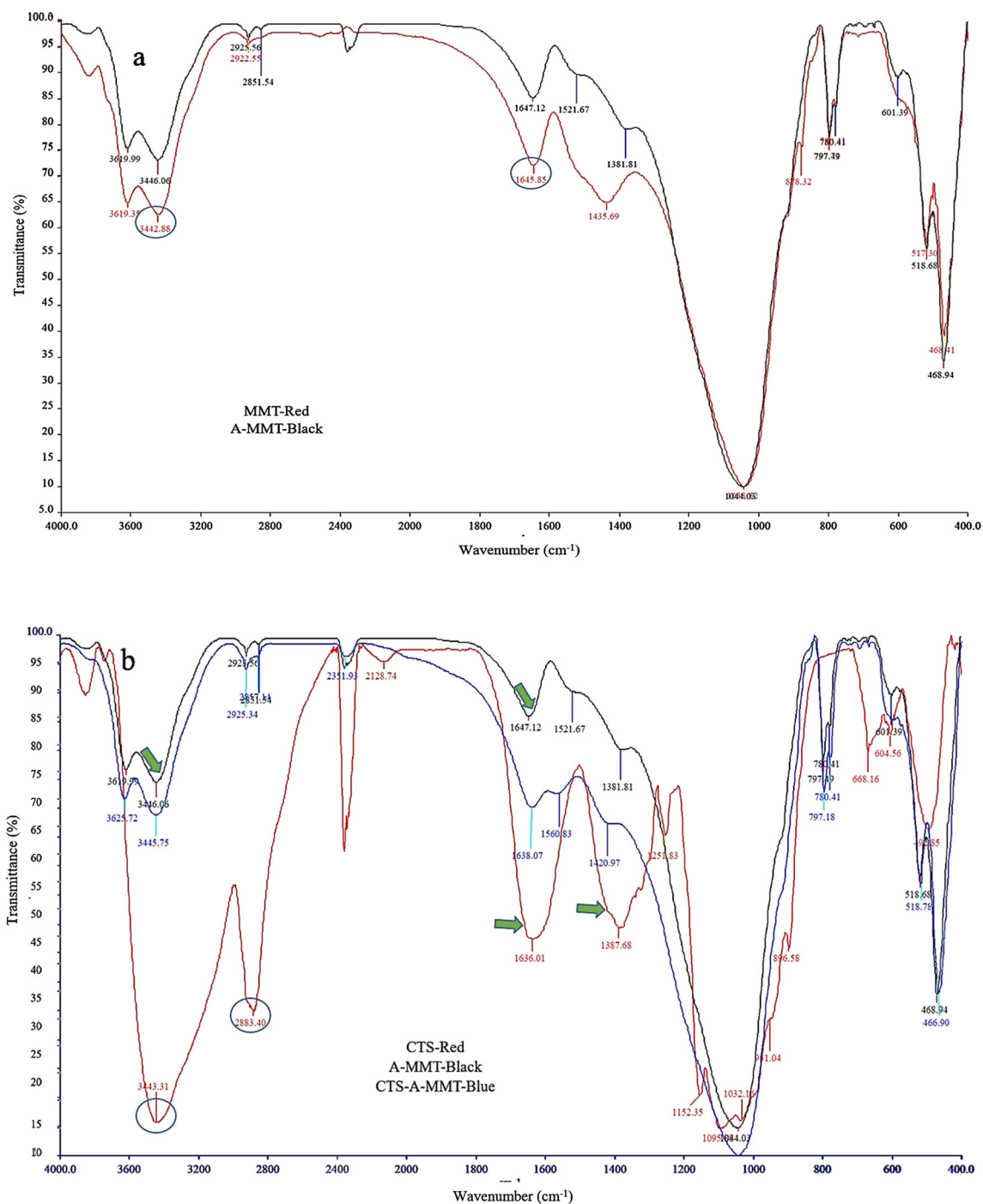


Fig. 2 FT-IR spectra. **a** Montmorillonite (red) and activated montmorillonite (black). **b** Chitosan (red), activated montmorillonite (black), and chitosan-activated montmorillonite composite (blue). **c** Chitosan-activated montmorillonite composite before (red) and after (black) metals

adsorption. **d** Chitosan-activated montmorillonite composite before (red) and after (black) oil adsorption. (For interpretation of the references to color in this figure legend, please see the web version of this article)

different sizes (Fig. 1b). As shown in Fig. 1c, A-MMT has a flaky and rough surface. Acid activation at high temperatures increases the porosity and changes the chemical composition of the clay, so that a portion of exchangeable cations such as calcium, potassium, and sodium, as well as iron and aluminum is reduced in the clay activation process (Table 1, Fig. S1). On the other hand, the Si content was

slightly increased after acid activation (Table 1). The possible reason is the lixiviation of Mg, Al, and Fe from MMT layers (Santos et al. 2015). Figure 1d shows CTS-A-MMT before adsorption process. Small flakes of A-MMT on the surface of chitosan are discernable. Similar morphological images are also reported by other authors who synthesized chitosan-clay composites (Auta and Hameed 2014; Saleh

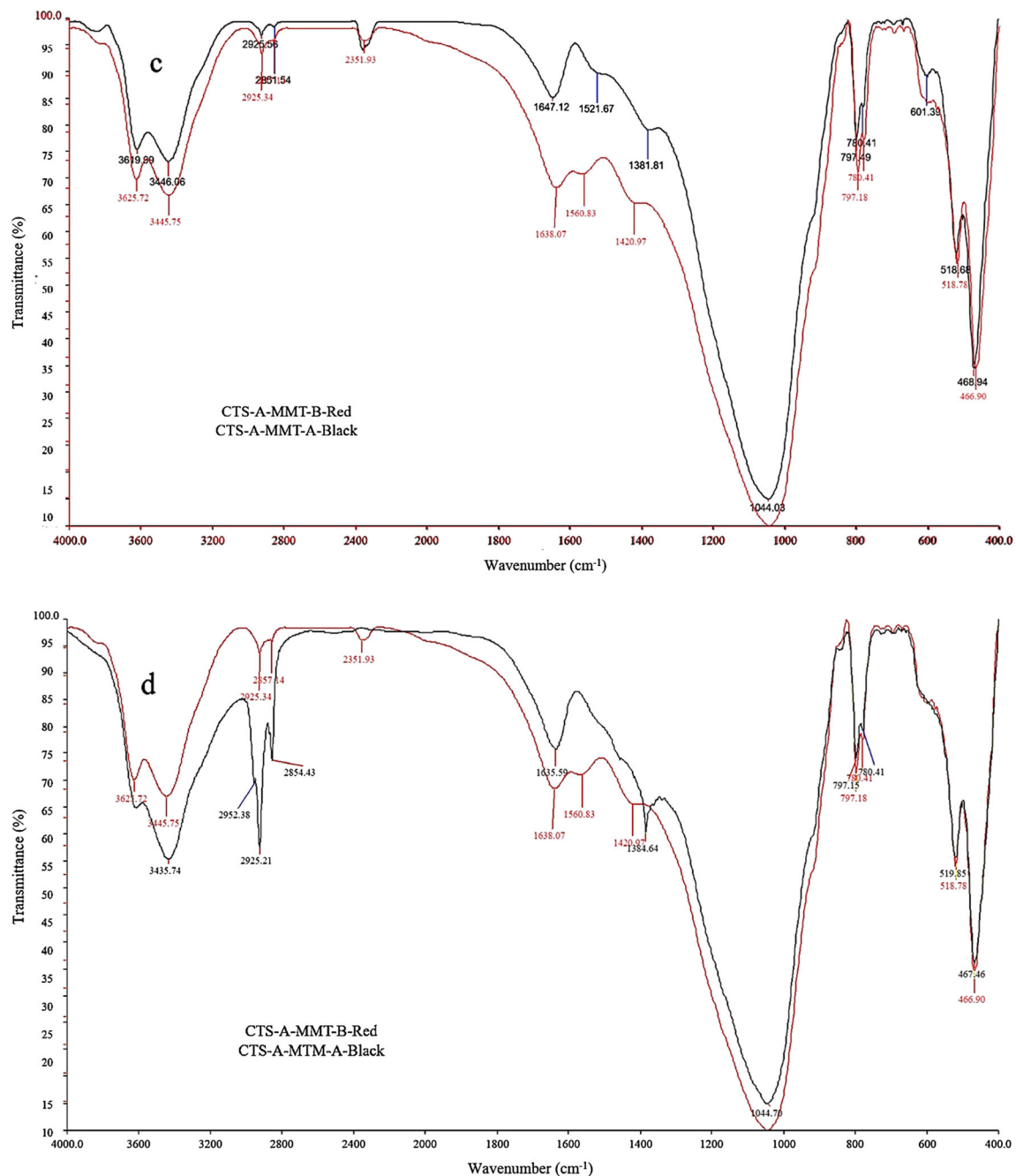


Fig. 2 (continued)

et al. 2016; Wan Ngah et al. 2013). Figure 1e and f illustrates the CTS-A-MMT composite after heavy metals, and oil adsorption, respectively. Clear morphological changes were observed after metals and oil adsorption process. The surface of CTS-A-MMT became smooth after adsorption of pollutants. These observations confirmed that metals and crude oil covered most of pores and active sites on the adsorbent surface after the adsorption process. In addition, the results of EDX analysis demonstrated that studied metals and crude oil were successfully adsorbed on CTS-A-MMT.

FT-IR analysis

The FT-IR spectrum of MMT before and after activation is presented in Fig. 2a. The original clay spectrum revealed absorption bands at 3442.88 and 1645.85 cm^{-1} assigned to the stretching and bending vibration of the $-\text{OH}$ groups, respectively. The raw clay composition changed considerably after acid treatment. Figure 2b shows the FT-IR spectra of CTS, A-MMT, and CTS-A-MMT. The IR spectra of CTS show an $-\text{OH}$ and $-\text{CH}$ stretching vibration at 3443.34 and 2883.40, respectively. Moreover, bands at around 1650 and

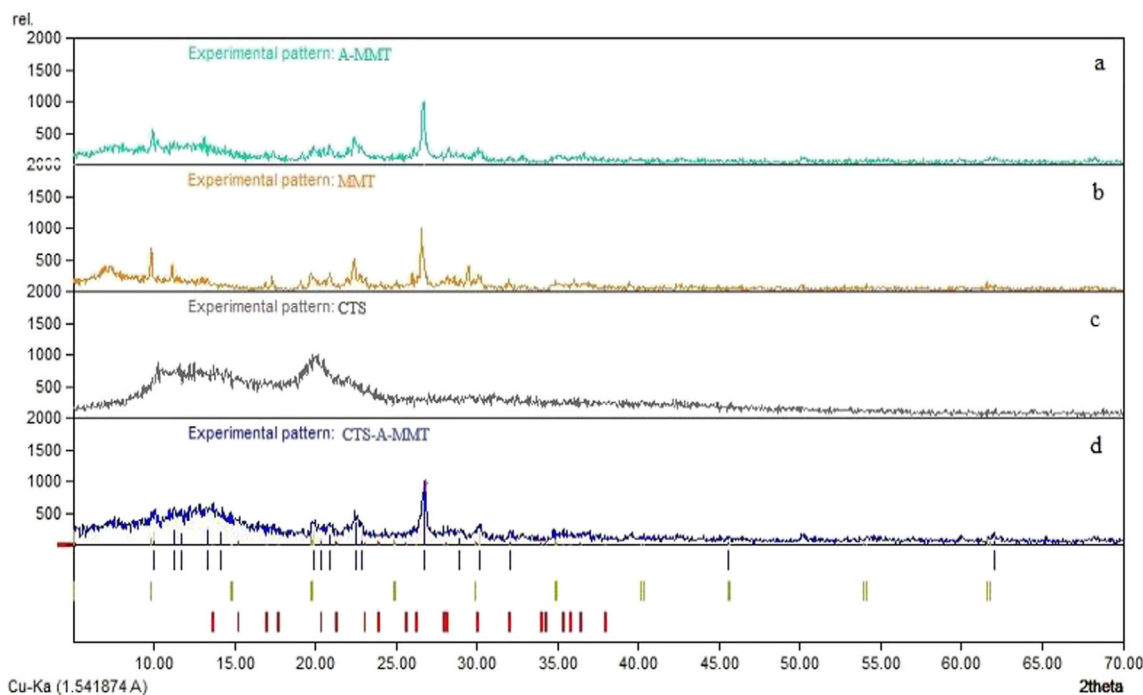


Fig. 3 X-ray diffraction (XRD) patterns of **a** A-MMT, **b** MMT, **c** CTS, and **d** CTS-A-MMT

1450 cm^{-1} represent the bending vibration of $-\text{NH}$ and $-\text{CH}_2$ groups, respectively. The 3400 and 1600 cm^{-1} bands for A-MMT are assigned to stretching and bending vibration of hydroxyl groups in molecular water present in A-MMT. Peaks around 800 and 480 cm^{-1} belong to Si-O in the tetrahedral sheet. As shown in Fig. 2b, the spectra of CTS-A-MMT occur between CTS and A-MMT spectra, reflecting the fact that CTS-A-MMT composite had an intermediate behavior between activated clay and chitosan beads. Moreover, two differences are exhibited between CTS-A-MMT composite and its predecessor material; (1) two new peaks appear at 2351.93 and 1560.83 cm^{-1} and (2) the position of $-\text{OH}$, $-\text{NH}$, and $-\text{CH}$ groups are shifted. Fig. 2, c and d, illustrate the spectra of CTS-A-MMT following metal ions and crude oil adsorption, respectively. Shifting and vibration of functional groups were detected on the CTS-A-MMT spectrum after

adsorption. Moreover, some post adsorption peaks were discerned on the spectrum of adsorbent.

XRD analysis

The XRD patterns of CTS, MMT, A-MMT, and CTS-A-MMT are presented in Fig. 3. The XRD of MMT indicated two peaks near $2\theta = 7.39^\circ$ and 26.66° corresponding to basal spacing of 11.96 and 3.34 Å, respectively (Fig. 3b). As shown in Fig. 3a, the intensity and width of the peaks were decreased and increased, respectively, following acid activation. Increase in the basal space indicates that the crystallinity of MMT is considerably affected by the acid activation. However, the inherent layered structure of MMT was not damaged in the process. The XRD pattern of CTS exhibited three peaks at around 10.29° , 13.76° , and 20.45°

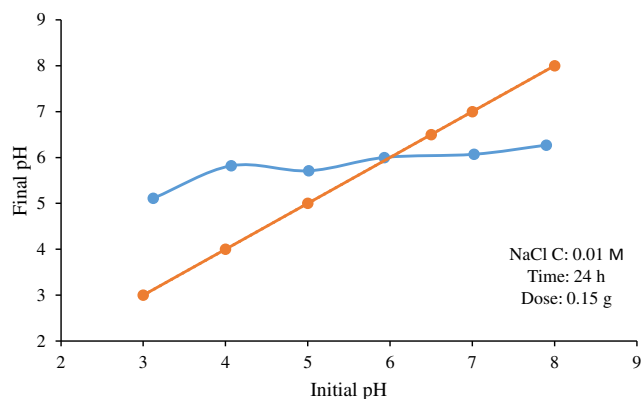


Fig. 4 Initial pH against final pH for determining pH_{pzc}

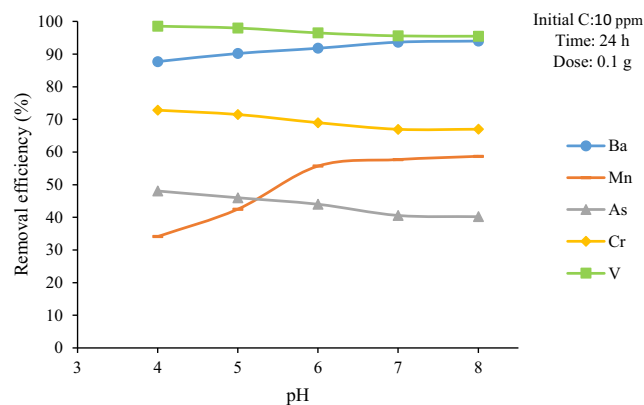
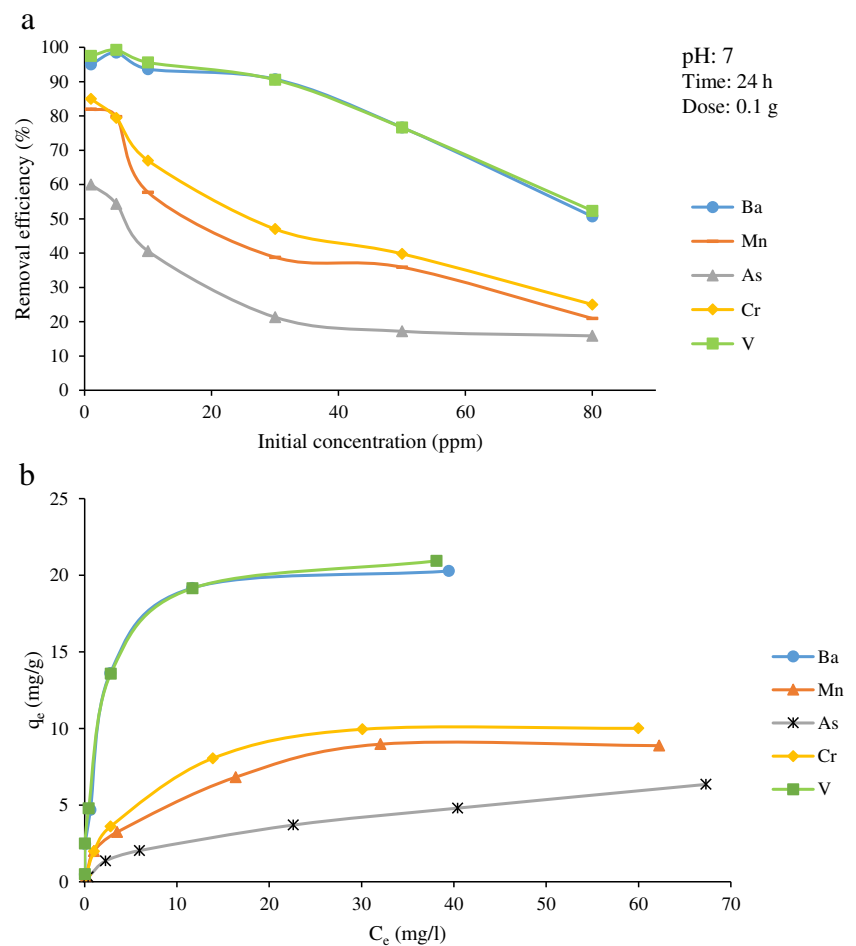


Fig. 5 Effect of pH on adsorption of heavy metal ions by CTS-A-MMT

Fig. 6 Percentage removal of the heavy metals at various initial concentrations (a), and isotherm curves of metals adsorption on the CTS-A-MMT biocomposite (b)



(Fig. 3c), while CTS-A-MMT, as shown in Fig. 3d, displayed significant changes in the intensity of the peaks. The main peaks at $2\theta = 13.36^\circ$ and 26.76° suggest the incorporation of A-MMT on the surface of CTS.

pH of point of zero charge (pH_{pzc})

A graph of initial pH versus final pH was plotted to determine the pH_{pzc} , (Fig. 4). Based on the results, the pH_{pzc} of CTS-A-MMT is 6.02. Hence, the surface charge of the adsorbent will be positive and negative if the pH value of the solution goes lower and

higher than pH_{pzc} , respectively. Hence, when pH of the solution is lower than pH_{pzc} , the adsorption of anions on CTS-A-MMT is favored, while the surface of CTS-A-MMT favors adsorption of cations when pH of the solution is above the pH_{pzc} .

Batch adsorption studies

pH effects

pH of a solution is generally taken as an important controlling parameter in adsorption studies because it affects both metals

Table 2 Langmuir, Freundlich, and Temkin constants along with correlation coefficients (R^2) for different metals

	Langmuir			Freundlich			Temkin		
	q_m (mg/g)	K_l (L/g)	R^2	$1/n$	K_f ((mg/g) (L/mg) $^{1/n}$)	R^2	K_T (L/mg)	bT (kJ/mol)	R^2
Ba	21.1416	0.0035	0.9984	0.5037	5.0487	0.8561	20.5323	0.7859	0.9524
Mn	9.2850	0.0691	0.9774	0.5196	1.4197	0.9469	4.4464	1.5446	0.9524
As	6.8027	0.2870	0.9578	0.5653	0.6427	0.9718	1.8802	2.2060	0.9215
Cr	11.0132	0.0468	0.9910	0.5333	1.6053	0.9510	4.8481	1.3665	0.9519
V	21.5054	0.0025	0.9989	0.4531	5.9016	0.8719	39.4052	0.8629	0.9584

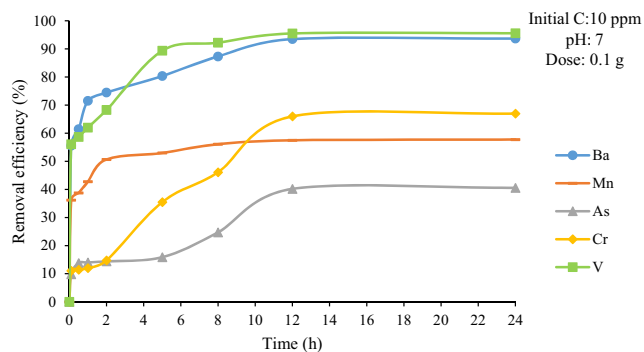


Fig. 7 Percentage removal of the heavy metals at various contact time

species and the surface charge of the adsorbent (Adamczuk and Kołodyńska 2015; Akhbarizadeh et al. 2014; Chai et al. 2016; Gogoi et al. 2016). Consequently, the surface chemistry of the solids highly influences the adsorption capacity and adsorption mechanisms (Assaad et al. 2007; Azzam et al. 2016; Moharami and Jalali 2013; Nestic et al. 2012). Figure 5 shows the adsorption results of Mn (II), Ba (II), As (III), V (V), and Cr (VI) on CTS-A-MMT at different pH (4–8). The results demonstrated that the pH of the metal solution affects the removal of metals. For instance, the removal percent of Mn was 34.1% and 57.8% at pH 4 and 8, respectively. Moreover, the removal percent of Mn (II) and Ba (II) increased with increasing pH. However, the adsorption of V, As, and Cr on CTS-A-MMT decreased with increasing pH. Such adsorption patterns are probably the result of a large number of binding sites on the surface functional groups of CTS-A-MMT, which become negatively and positively charged at higher and lower pH than 6.02 (pH_{pzc}), respectively. At low pH, most of the amine groups of CTS in the CTS-A-MMT were ionized and presented as $-NH^{3+}$; hence, electrostatic repulsion between cations and $-NH^{3+}$ may prevent the adsorption of cations onto the adsorbent (Azzam et al. 2016; Cho et al. 2012). On the other hand, low adsorption efficiency of anions at higher pH values can be attributed to the negative surface charge of adsorbent as well as shifted metals speciation (Cho et al. 2012; Saleh et al. 2016). Thus, the electrostatic repulsion between the metals and the edge group with negative and positive charge and chemical speciation of metal ions at different pH restricts metal access to the surface binding sites and finally will affect the adsorption efficiency (Cho et al. 2012; Gogoi et al. 2016; Pawar et al. 2016; Taha et al. 2016). The positively and negatively charged metal ions also compete with the high concentration of H^+ and OH^- ions in the solution (Pawar et al. 2016; Taha et al. 2016; Wan Ngah et al. 2012). The percentage removal of all metals remained almost constant beyond pH 7.0.

Effects of the initial concentration

The effects of initial metals concentration were investigated by changing the concentration from 1 to 80 mg/L at pH of 7.0

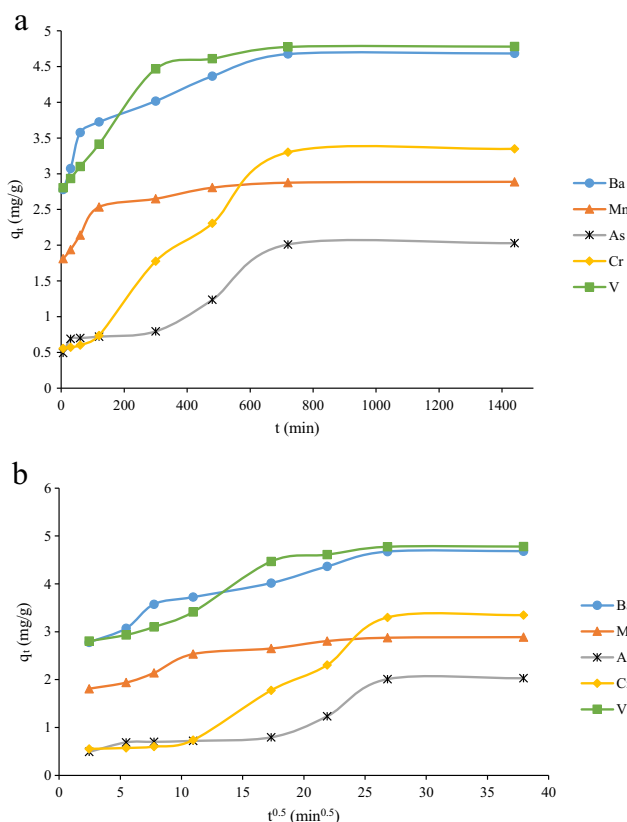


Fig. 8 Plots of the a kinetic curves and b intra-particle diffusion curve for adsorption of metal ions onto CTS-A-MMT

for 24 h (Fig. 6a). The results demonstrated that high removal efficiency at low metal concentration decreases gradually with increasing initial concentration. Considering the fact that active sites of adsorbent are constant during the increasing of initial concentration (Pawar et al. 2016), these results were expected. The slope of the removal efficiency curve for Ba and V is less than the other metals. The possible reason is the higher adsorbent affinity for Ba and V in higher concentrations.

Adsorption isotherms describe how metal ions interact with an adsorbent (Wan Ngah et al. 2012; Wang et al. 2014a). The concentration data were analyzed using adsorption isotherms (Fig. 6b). The calculated constant and the correlation coefficient (R^2) values for Langmuir, Freundlich, and Temkin isotherms are presented in Table 2. The R^2 value for all metals (except As) in Langmuir model is higher than the other two isotherms. This suggests that the adsorption of V, Ba, Cr, and Mn occurred through monolayer formation and the similar active sites were involved in the removal process. Langmuir model did not fit very well for As, while the experimental data of As fitted better with Freundlich isotherm. This shows that the As adsorption on CTS-A-MMT surface was heterogeneous. Furthermore, the Langmuir monolayer capacity (q_e) of the studied metals displays the following decreasing trend: V (21.50) > Ba (21.14) > Cr (11.01) > Mn (9.28) > As (6.80).

Table 3 Values of kinetic parameters for pseudo-first-order and pseudo-second-order models

	Pseudo-first-order model			Pseudo-second-order model		
	k_1 (min ⁻¹)	q_e (mg/g)	R^2	K_2 (g/mg/min)	q_e (mg/g)	R^2
Ba (II)	0.0065	2.0583	0.8654	0.0083	4.7483	0.9988
Mn (II)	0.0059	1.0580	0.9771	0.0200	2.9197	0.9997
As (III)	0.0050	2.0092	0.7137	0.0022	2.2172	0.8827
Cr (VI)	0.0050	3.3038	0.8268	0.0009	4.0064	0.9098
V (V)	0.0082	2.7471	0.9432	0.0061	4.9068	0.9980

The higher values of q_e commonly demonstrate the affinity of adsorbent to the metal ion (Pawar et al. 2016; Taha et al. 2016). K_f and $1/n$ give information on the extent of adsorption and the adsorption intensity, respectively (Auta and Hameed 2013). Besides pH, differences in the percentage removal of various metals are believed to be the result of physio-chemical properties, the initial concentration, ionic radius, and the electronegativity of metal ions, and also the ionic strength of the solution (Akhbarizadeh et al. 2014; Pawar et al. 2016).

Effects of the contact time

Investigating the percentage removal with time provided useful information regarding the rate of treatment time and the time at which adsorption equilibrium occurs (Pawar et al. 2016). The optimal treatment time leads to reduction of capital

and operation cost (Taha et al. 2016). Figure 7 illustrates the percentage removal of Mn (II), Ba (II), As (III), V (V), and Cr (VI) at different time intervals ranging from 6 min to 24 h. The pH of the solution was kept constant at 7.0. The results showed that an increase in contact time (until 12 h) favors the uptake of metals from solution. However, the adsorption rate for the five metal ions differs. A very fast adsorption rate was observed within the first 2 h. In addition, increasing contact time was accompanied with slow increase in percentage removal of metals and finally, equilibrium was achieved within 12 h. These observations probably reflect the availability of the adsorbent surface area, a large number of void binding sites, and good functional groups on adsorbent at initial stages (Bhattacharyya and Gupta 2008; Taha et al. 2016).

In order to clarify the controlling steps of mass transfer and chemical reaction (Wang et al. 2014a), the sorption experimental data were analyzed using pseudo-first-order-kinetic and pseudo-second-order kinetic models. The plots of the $\ln(q_e - q_t)$ versus t (min) and t/q_t versus t (min) for the pseudo-first-order-kinetic and pseudo-second-order kinetic models, respectively, are shown in Fig. 8a. Moreover, Table 3 displays the calculated constants (k_1 and k_2), the adsorption capacity (q_e), and the correlation coefficients (R^2). The results exhibited a better fit to the pseudo-second-order kinetic model with R^2 values of 0.9988, 0.9997, 0.8827, 0.9098, and 0.9980 for Ba (II), Mn (II), As (III), Cr (VI), and V (V), respectively. This suggests that the chemisorption (chemical bond formation

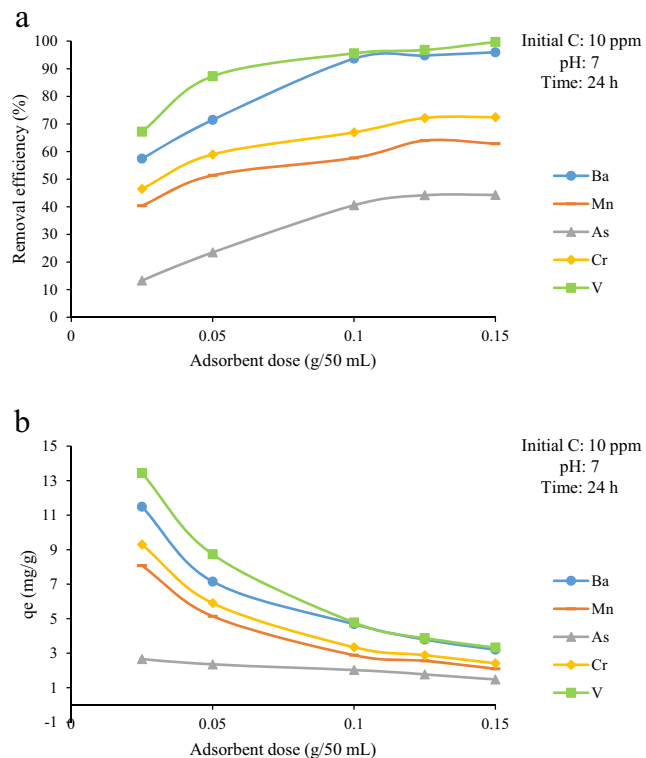


Fig. 9 Adsorbent dose effects on the percentage removal of metal ions (a) and adsorption capacity of adsorbent (b)

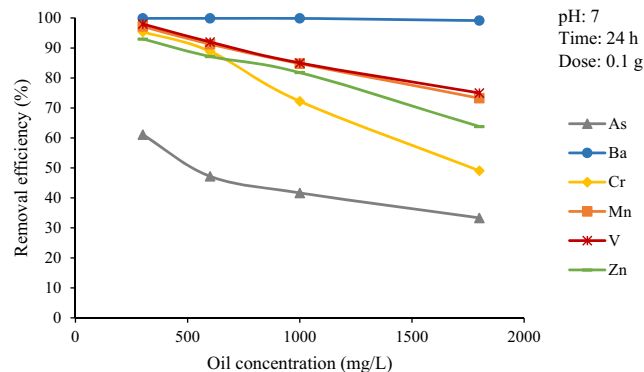


Fig. 10 Effects of the oil presence on the removal of metal ions. The initial concentration of Ba, Mn, As, Zn, Cr, and V was 5.8, 3.55, 0.18, 0.6, 0.1, and 0.1 mg/L respectively

Table 4 Langmuir, Freundlich, and Temkin constants along with correlation coefficients (R^2) for crude oil adsorption on CTS-A-MMT

Langmuir			Freundlich			Temkin		
q_m (mg/g)	K_1 (L/g)	R^2	$1/n$	$K_f((\text{mg/g}) (\text{L/mg})^{1/n})$	R^2	K_T (L/mg)	bT (kJ/mol)	R^2
344.8276	0.0095	0.9942	0.1525	104.29	0.9878	1.9067	0.0624	0.9681

between the adsorbent and adsorbate molecule) is the possible rate-controlling step of the process (Doshi et al. 2018).

Since the adsorbent has porous nature, the intra-particle diffusion model was also carried out in order to check the relative significance of intra-particle (pore) diffusion and boundary layer (film) diffusion for metals adsorption (Fig. 8b). The multi-linear plot during the sorption process demonstrates three regions for metals that indicate that two or more steps influenced the adsorption process. The first linear step describes the surface or film diffusion. In this stage, adsorption takes place on surface of adsorbent until saturation of exterior surface by metal ions. The second linear step represents the gradual inward diffusion stage; hence, metal ions were adsorbed into pores of adsorbents within the particle. The tired region, which is the slowest stage, demonstrates the final equilibrium between the remained metal ions in the solution and the adsorbed ions. In this stage, the pore volume of adsorbent decreases, so the intra-particle or pore diffusion decreased. Hence, the early stage of adsorption process is controlled by the film diffusion and/ or surface reactions, while pore diffusion controls the next stages. Similar results were reported by previous studies (Doshi et al. 2018; Negm et al. 2015; Pawar et al. 2016; Taha et al. 2016).

Effects of the adsorbent dose

It is obvious that the percentage removal of heavy metals increases with addition of the adsorbent dose (Taha et al. 2016).

However, it is important to determine the optimal dosage that maximizes the removal efficiency without increasing operational cost. In this study, the effects of CTS-A-MMT were studied by varying the adsorbent dose from 0.025 to 0.15 g/50 mL. As shown in Fig. 9a, the percentage removal of heavy metals increased fastly from 0.025 to 0.1 g/50 mL, and then started to slow down. The reason is probably limited available vacant sites at the lower dose. However, the adsorption capacity (q_e) decreased as the adsorbent dose increased (Fig. 9b). The possible reasons are (1) coming down the number of covered sites per unit mass due to the saturation reduction of the adsorption sites and (2) particles aggregation as a result of higher sorbent amounts (Saleh et al. 2016; Taha et al. 2016).

Effects of the presence of crude oil

The percentage removal of Mn (II), Ba (II), As (III), V (V), Zn (II), and Cr (VI) was also investigated in the presence of crude oil with initial concentrations of 300 to 1800 mg/L at pH 7. Furthermore, the initial concentration of the studied metals in synthetic solution was approximately close to their concentration in real PW from the Persian Gulf. Accordingly, the concentrations of Ba, Mn, As, Zn, Cr, and V proved to be 5.8, 3.55, 0.18, 0.16, 0.1, and 0.1 mg/L respectively. As depicted in Fig. 10, increasing the initial oil concentration notably decreased the uptake of all metals especially Cr (VI) and As (III). However, at 600 mg/L oil concentration (the concentration of

Fig. 11 Oil adsorption versus different adsorbent dose. Lines are the standard values of PW discharge to environment in different parts of the world

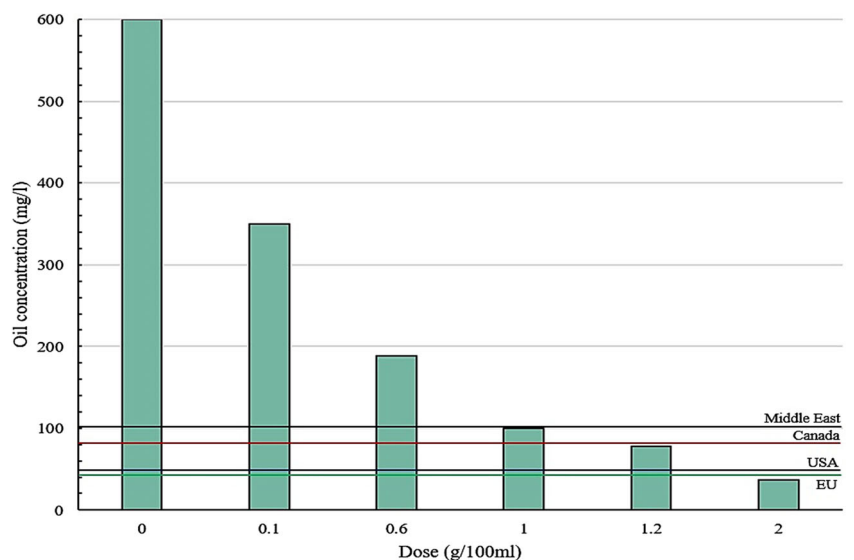


Table 5 Salinity, pH, and metals concentration of produced water sample from the Persian Gulf and worldwide ocean discharge criteria

		pH	Salinity (g/L)	V ($\mu\text{g/L}$)	Cr ($\mu\text{g/L}$)	Mn ($\mu\text{g/L}$)	Zn ($\mu\text{g/L}$)	As ($\mu\text{g/L}$)	Ba ($\mu\text{g/L}$)	Reference
Produced water, Iran	Before treatment	7.83	42.5	50	38.9	2690	527	168.4	5380	This study
	After treatment	7.5	30.34	12	< 0.05	1212.50	10	24	1356	
Ocean discharge criteria	Iran	6.5–8.5	*	100	1000	1000	2000	100	5000	(Department of Environment, I. R. Iran 2013)
	USA	6.5–9	35	–	–	200	95	69	–	(Jones et al. 2000; USEPA 1993)
	England	6.5–8.5	–	–	50	–	300	50	–	(Robinson 2013; Shpiner et al. 2009b)

*Increase up to 10% of salinity of the discharge area is acceptable

crude oil in the real PW sample), more than 80% of Ba, Mn, Cr, Zn, and V, and over 40% of As was removed.

The mechanism of oil removal was investigated using Langmuir, Freundlich, and Temkin adsorption isotherms. Table 4 demonstrates the calculated constant and correlation coefficient (R^2) values for different isotherm. Based on the results, the R^2 value in Langmuir model is higher. Hence, oil adsorption to CTS-A-MMT seems to follow the monolayer model.

The percentage removal of oil from synthetic solution was investigated by varying CTS-A-MMT dose from 0.1 to 2 g. The initial oil concentration, volume of solution, pH, and contact time were 600 mg/L, 100 mL, 7, and 24 h, respectively (Fig. 11). Clearly, the removal percentage of oil increases with adding the adsorbent dose, and after using 2 g CTS-A-MMT in 100 mL solution, the oil concentration decreased to 37 mg/L, which is lower than the maximum permissible limit in Canada (80 mg/L), Middle East (100 mg/L), Europe (40 mg/L), and the USA (42 mg/L) (Ahmad and Baddour 2014; Jones et al. 2000; Robinson 2013).

Treatment of produced water

Treatment of produced water (PW) is an effective option for its handling, after which, it has the potential to become a valuable product rather than a waste (Arthur et al. 2005). In this study, CTS-A-MMT was applied to

remove metal ions and crude oil from PW. For this purpose, PW samples were collected from oil storing tanks in Khark Island, Persian Gulf, Iran. Salinity, pH, and metal concentration of collected PW were measured before treatment (Table 5). Experiments were performed using 100 mL of raw PW. The adsorbent dose was increased from 0.2 to 1.2 g/100 mL, and the contact time was 24 h. As expected, the removal efficiency of pollutants increased with increasing dose of CTS-A-MMT, and the color of the wastewater changed from brown to colorless (Fig. 12). The concentration of heavy metals in the wastewater was measured at each step. As shown in Fig. 13, the presence of competing ions in PW brine sample notably decreased the uptake of As (III), Ba (II), Cr (VI), Mn (II), V (V), and Zn (II) from solution by CTS-A-MMT. However, the removal efficiency of metal ions within 24 h using 1.2 g/100 mL of adsorbent exceeded 60% (Fig. 13 and Table 5). In addition, metal concentration in treated wastewater became much lower than the ocean discharge criteria (Table 5).

Conclusion

In this study, a new protocol was developed to obtain a novel low-cost bio-adsorbent from shrimp shell and naturally

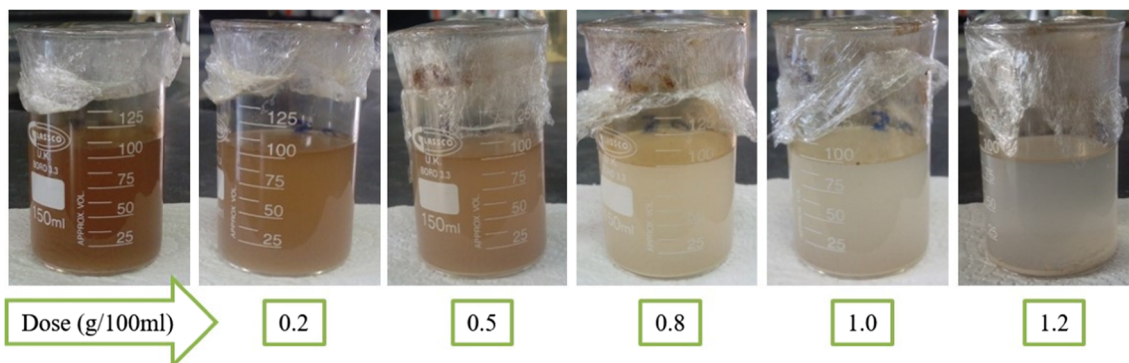


Fig. 12 Treatment of PW with different doses of CTS-A-MMT

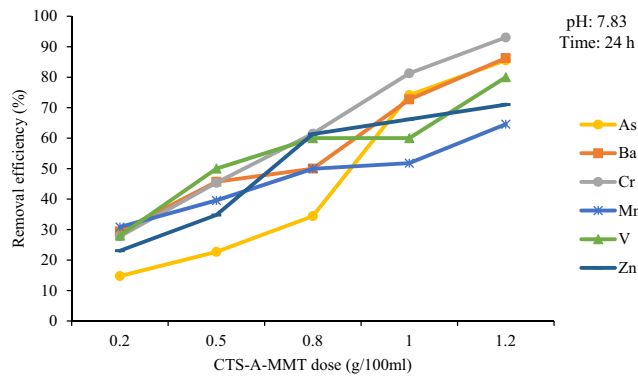


Fig. 13 Removal efficiency of the As (III), Ba (II), Cr (VI), Mn (II), V (V), and Zn (II) in PW sample with different adsorbent doses and in the presence of other ions and crude oil

occurring montmorillonite, activated by acid under mild synthetic conditions. The results revealed that CTS-A-MMT could be applied efficiently for simultaneous removal of crude oil (over 87% recovery) and heavy metals (65–93% recovery range) from PW. The obtained high removal efficiencies open a new perspective for the application of CTS-A-MMT in the oil industry. Economically, the final cost for PW treatment using CTS-A-MMT is estimated to be 0.02 \$/bbl, which is much lower than the presently used methods. Moreover, high degradability and recyclability of the synthesized adsorbent makes it eco-friendly.

Acknowledgments The authors would like to express their gratitude to medical geology research center of Shiraz University for logistic support. Thanks are also extended to the Iranian Oil Terminal Company for facilitating the fieldwork and financially supporting this research.

References

Adamczuk A, Kolodyńska D (2015) Equilibrium, thermodynamic and kinetic studies on removal of chromium, copper, zinc and arsenic from aqueous solutions onto fly ash coated by chitosan. *Chem Eng J* 274:200–212

Ahmad N, Baddour RE (2014) A review of sources, effects, disposal methods, and regulations of brine into marine environments. *Ocean Coast Manag* 87:1–7

Akhbarizadeh R, Shayestefar MR, Darezereshki E (2014) Competitive removal of metals from wastewater by maghemite nanoparticles: a comparison between simulated wastewater and AMD. *Mine Water Environ* 33:89–96

Arthur JD, Langhus BG, Patel C (2005) Technical summary of oil and gas produced water treatment technologies. All Consulting, LLC, Tulsa

Assaad E, Azzouz A, Nistor D, Ursu AV, Sajin T, Miron DN, Monette F, Niquette P, Hausler R (2007) Metal removal through synergic coagulation–flocculation using an optimized chitosan–montmorillonite system. *Appl Clay Sci* 37:258–274

Auta M, Hameed BH (2013) Coalesced chitosan activated carbon composite for batch and fixed-bed adsorption of cationic and anionic dyes. *Colloids Surf B Biointerfaces* 105:199–206

Auta M, Hameed BH (2014) Chitosan–clay composite as highly effective and low-cost adsorbent for batch and fixed-bed adsorption of methylene blue. *Chem Eng J* 237:352–361

Azzam EM, Eshaq G, Rabie AM, Bakr AA, Abd-Elal AA, El Metwally AE, Tawfik SM (2016) Preparation and characterization of chitosan-clay nanocomposites for the removal of Cu(II) from aqueous solution. *Int J Biol Macromol* 89:507–517

Bhattacharyya KG, Gupta SS (2008) Influence of acid activation on adsorption of Ni(II) and Cu(II) on kaolinite and montmorillonite: kinetic and thermodynamic study. *Chem Eng J* 136:1–13

Chai L, Yue M, Yang J, Wang Q, Li Q, Liu H (2016) Formation of tooeelite and the role of direct removal of As(III) from high-arsenic acid wastewater. *J Hazard Mater* 320:620–627

Chen L, Wu P, Chen M, Lai X, Ahmed Z, Zhu N, Dang Z, Bi Y, Liu T (2018) Preparation and characterization of the eco-friendly chitosan/vermiculite biocomposite with excellent removal capacity for cadmium and lead. *Appl Clay Sci* 159:74–82

Cho D-W, Jeon B-H, Chon C-M, Kim Y, Schwartz FW, Lee E-S, Song H (2012) A novel chitosan/clay/magnetite composite for adsorption of Cu(II) and As(V). *Chem Eng J* 200–202:654–662

da Costa MP, de Mello Ferreira IL, de Macedo Cruz MT (2016) New polyelectrolyte complex from pectin/chitosan and montmorillonite clay. *Carbohydr Polym* 146:123–130

de Queiroga LNF, Soares PK, Fonseca MG, de Oliveira FJVE (2016) Experimental design investigation for vermiculite modification: intercalation reaction and application for dye removal. *Appl Clay Sci* 126:113–121

Department of Environment (2013) Environmental Procedure. Environmental Regulations And Standards, Islamic Republic of Iran (In Persian)

Djukić A, Jovanović U, Tuvic T, Andrić V, Novaković JG, Ivanović N, Matović L (2013) The potential of ball-milled Serbian natural clay for removal of heavy metal contaminants from wastewaters: simultaneous sorption of Ni, Cr, Cd and Pb ions. *Ceram Int* 39:7173–7178

Doshi B, Ayati A, Tanhaei B, Repo E, Sillanpää M (2018) Partially carboxymethylated and partially cross-linked surface of chitosan versus the adsorptive removal of dyes and divalent metal ions. *Carbohydr Polym* 197:586–597

Dotto GL, Rodrigues FK, Tanabe EH, Fröhlich R, Bertuol DA, Martins TR, Foletto EL (2016) Development of chitosan/bentonite hybrid composite to remove hazardous anionic and cationic dyes from colored effluents. *J Environ Chem Eng* 4:3230–3239

Du Y, Zhao Y, Dai S, Yang B (2009) Preparation of water-soluble chitosan from shrimp shell and its antibacterial activity. *Innov Food Sci Emerg Technol* 10:103–107

El-Dib FI, Tawfik FM, Eshaq G, Hefni HH, ElMetwally AE (2016) Remediation of distilleries wastewater using chitosan immobilized bentonite and bentonite based organoclays. *Int J Biol Macromol* 86:750–755

Fakhru’l-Razi A, Pendashteh A, Abdullah LC, Biak DR, Madaeni SS, Abidin ZZ (2009) Review of technologies for oil and gas produced water treatment. *J Hazard Mater* 170:530–551

Farag AM, Harper DD (2014) A review of environmental impacts of salts from produced waters on aquatic resources. *Int J Coal Geol* 126:157–161

Futalan CM, Kan C-C, Dalida ML, Hsien K-J, Pascua C, Wan M-W (2011) Comparative and competitive adsorption of copper, lead, and nickel using chitosan immobilized on bentonite. *Carbohydr Polym* 83:528–536

Gogoi P, Thakur AJ, Devi RR, Das B, Maji TK (2016) A comparative study on sorption of arsenate ions from water by crosslinked chitosan and crosslinked chitosan/MMT nanocomposite. *J Environ Chem Eng* 4:4248–4257

Hadjiltaief HB, Sdiri A, Ltaief W, Da Costa P, Galvez ME, Zina MB (2018) Efficient removal of cadmium and 2-chlorophenol in aqueous systems by natural clay: adsorption and photo-fenton degradation processes. *CR Chim* 21:253–262

- Hu C, Deng Y, Hu H, Duan Y, Zhai K (2016) Adsorption and intercalation of low and medium molar mass chitosans on/in the sodium montmorillonite. *Int J Biol Macromol* 92:1191–1196
- Iler KR (1979) The chemistry of silica. Solubility, polymerization, colloid and surface properties and biochemistry of silica. Wiley, New York
- Jones F, Leuterman A, Still I (2000) Discharge practices and standards for offshore operations around the world, proceedings of the 7th International Petroleum Environmental Conference, Albuquerque, NM 903–938
- Luo X, Zeng J, Liu S, Zhang L (2015) An effective and recyclable adsorbent for the removal of heavy metal ions from aqueous system: magnetic chitosan/cellulose microspheres. *Bioresour Technol* 194:403–406
- Moharami S, Jalali M (2013) Removal of phosphorus from aqueous solution by Iranian natural adsorbents. *Chem Eng J* 223:328–339
- Negm NA, El Sheikh R, El-Faragy AF, Hefni HHH, Bekhit M (2015) Treatment of industrial wastewater containing copper and cobalt ions using modified chitosan. *J Ind Eng Chem* 21:526–534
- Nesic AR, Velickovic SJ, Antonovic DG (2012) Characterization of chitosan/montmorillonite membranes as adsorbents for Bezactiv Orange V-3R dye. *J Hazard Mater* 209–210:256–263
- Olsson O, Weichgrebe D, Rosenwinkel K-H (2013) Hydraulic fracturing wastewater in Germany: composition, treatment, concerns. *Environ Earth Sci* 70:3895–3906
- Pawar RR, Lalmunsiam, Bajaj HC, Lee S-M (2016) Activated bentonite as a low-cost adsorbent for the removal of Cu(II) and Pb(II) from aqueous solutions: batch and column studies. *J Ind Eng Chem* 34:213–223
- Phan TT, Capo RC, Stewart BW, Graney JR, Johnson JD, Sharma S, Toro J (2015) Trace metal distribution and mobility in drill cuttings and produced waters from Marcellus Shale gas extraction: uranium, arsenic, barium. *Appl Geochem* 60:89–103
- Robinson D (2013) Oil and gas: treatment and discharge of produced waters onshore. *Filtr Separat* 50:40–46
- Saleh TA, Sari A, Tuzen M (2016) Chitosan-modified vermiculite for As(III) adsorption from aqueous solution: equilibrium, thermodynamic and kinetic studies. *J Mol Liq* 219:937–945
- Santos SSG, Silva HRM, de Souza AG, Alves APM, da Silva Filho EC, Fonseca MG (2015) Acid-leached mixed vermiculites obtained by treatment with nitric acid. *Appl Clay Sci* 104:286–294
- Sargin I, Kaya M, Arslan G, Baran T, Ceter T (2015) Preparation and characterisation of biodegradable pollen–chitosan microcapsules and its application in heavy metal removal. *Bioresour Technol* 177:1–7
- Shankar P, Gomathi T, Vijayalakshmi K, Sudha P (2014) Comparative studies on the removal of heavy metals ions onto cross linked chitosan-g-acrylonitrile copolymer. *Int J Biol Macromol* 67:180–188
- Shpiner R, Liu G, Stuckey D (2009a) Treatment of oilfield produced water by waste stabilization ponds: biodegradation of petroleum-derived materials. *Bioresour Technol* 100:6229–6235
- Shpiner R, Vathi S, Stuckey DC (2009b) Treatment of oil well “produced water” by waste stabilization ponds: removal of heavy metals. *Water Res* 43:4258–4268
- Skalak KJ, Engle MA, Rowan EL, Jolly GD, Conko KM, Benthem AJ, Kraemer TF (2014) Surface disposal of produced waters in western and southwestern Pennsylvania: potential for accumulation of alkali-earth elements in sediments. *Int J Coal Geol* 126:162–170
- Song X, Li L, Zhou L, Chen P (2018) Magnetic thiolated/quaternized-chitosan composites design and application for various heavy metal ions removal, including cation and anion. *Chem Eng Res Des* 136:581–592
- Stawinski W, Freitas O, Chmielarz L, Wegrzyn A, Komadera K, Blachowski A, Figueiredo S (2016) The influence of acid treatments over vermiculite based material as adsorbent for cationic textile dyes. *Chemosphere* 153:115–129
- Taha AA, Shreadah MA, Ahmed AM, Heiba HF (2016) Multi-component adsorption of Pb(II), Cd(II), and Ni(II) onto Egyptian Na-activated bentonite; equilibrium, kinetics, thermodynamics, and application for seawater desalination. *J Environ Chem Eng* 4:1166–1180
- Torres L, Yadav OP, Khan E (2017) Holistic risk assessment of surface water contamination due to Pb-210 in oil produced water from the Bakken Shale. *Chemosphere* 169:627–635
- USEPA (1993) Final Development Document for Effluent Limitations Guidelines and New Source Performance Standards for the Offshore Subcategory of the Oil and Gas Extraction Point Source category. EPA 821-R-93-003. U.S. Environmental Protection Agency, Office of Water, Washington, DC
- USEPA E (1999) Method 1664 revision A: N-hexane extractable material (HEM; oil and grease) and silica gel treated N-hexane extractable material (SGT-HEM; non-polar material) by extraction and gravimetry. United States Environmental Protection Agency, Washington DC
- Venkatesan A, Wankat PC (2017) Produced water desalination: an exploratory study. *Desalination* 404:328–340
- Vieira RM, Vilela PB, Becegato VA, Paulino AT (2018) Chitosan-based hydrogel and chitosan/acid-activated montmorillonite composite hydrogel for the adsorption and removal of Pb + 2 and Ni + 2 ions accommodated in aqueous solutions. *J Environ Chem Eng* 6:2713–2723
- Wan Ngah WS, Teong LC, Toh RH, Hanafiah MAKM (2012) Utilization of chitosan–zeolite composite in the removal of Cu(II) from aqueous solution: adsorption, desorption and fixed bed column studies. *Chem Eng J* 209:46–53
- Wan Ngah WS, Teong LC, Toh RH, Hanafiah MAKM (2013) Comparative study on adsorption and desorption of Cu(II) ions by three types of chitosan–zeolite composites. *Chem Eng J* 223:231–238
- Wang H, Tang H, Liu Z, Zhang X, Hao Z, Liu Z (2014a) Removal of cobalt(II) ion from aqueous solution by chitosan-montmorillonite. *J Environ Sci (China)* 26:1879–1884
- Wang X, Yang L, Zhang J, Wang C, Li Q (2014b) Preparation and characterization of chitosan–poly(vinyl alcohol)/bentonite nanocomposites for adsorption of Hg(II) ions. *Chem Eng J* 251:404–412
- Zhang L, Zeng Y, Cheng Z (2016) Removal of heavy metal ions using chitosan and modified chitosan: a review. *J Mol Liq* 214:175–191